Available online at www.sciencedirect.com
SCIENCE DIRECT®
Journal of Magnetic Resonance 160 (2003) 144–150
JMR Journal of Magnetic Resonance
www.elsevier.com/locate/jmr

Multipoint mapping for imaging of semi-solid materials

M.A. Fernández-Seara,[a] S.L. Wehrli,[b] and F.W. Wehrli[a,*]

[a] *Laboratory for Structural NMR Imaging, Department of Radiology, University of Pennsylvania, Philadelphia, PA, USA*
[b] *NMR Core Facility, Children Hospital, Philadelphia, PA, USA*

Received 2 August 2002; revised 29 October 2002

Abstract

Multipoint *k*-space mapping is a hybrid between constant-time (single-point mapping) and spin-warp imaging, involving sampling of a *k*-line segment of **r** points per TR cycle. In this work the method was implemented for NMR imaging of semi-solid materials on a 400 MHz micro-imaging system and two different *k*-space sampling strategies were investigated to minimize the adverse effects from relaxation-induced *k*-space signal modulation. Signal attenuation from T_2 decay results in artifacts whose nature depends on the *k*-space sampling strategy. The artifacts can be minimized by increasing the readout gradient amplitude, by PSF deconvolution or by oversampling in readout direction. Finally, implementation of a T_2 selective RF excitation demonstrates the feasibility of obtaining short-T_2 contrast even in the presence of tissues with long-T_2. The method's potential is illustrated with 3D proton images of short-T_2 materials such as synthetic polymers and bone.

Keywords: MRI; Pulse sequence; Multipoint mapping; Solids imaging; Short-T_2 contrast

1. Introduction

The single *k*-space point mapping technique (SPI), conceived by Emid and Creyghton [1], has been widely used for imaging of heterogeneous broad line-width materials [2–4] since it allows for short effective echo times. Moreover, because each *k*-space point is sampled at equal time during signal evolution, images can be acquired that are free of susceptibility, chemical shift, and inhomogeneous B_0 field effects. However, the sequence is inherently inefficient and scan times can become excessive for large data matrices.

Several modifications of SPI have been proposed that use pure phase encoding techniques combined with EPI [5] or RARE-type [6] acquisitions in order to speed up the data collection while maintaining the ability of SPI to acquire artifact-free images. These sequences are appropriate for imaging materials with short-T_2^* but relatively long-T_2, since sampling is done at the echo maxima of a spin echo train, and therefore the signal decay at sampling times is determined by T_2, since T_2^* relaxation is refocused. The effective echo time of these sequences, however, is too long for imaging of materials with intrinsically short-T_2.

Cho and Ro [7] first proposed what they referred to as 'multipoint (MP) *k*-space mapping,' an extension of the original SPI technique to reduce the scan time by an integer factor **r**, achieved by sampling the *k*-space lines in a piecewise fashion. To the best of our knowledge, however, this method has not been reduced to practice yet, except in the form of preliminary work done in the authors' laboratory [8]. In this work we have implemented a MP mapping sequence, investigated two different *k*-space trajectories, studied the effects of T_2^* decay by point-spread function (PSF) analysis and demonstrated the method's potential for proton imaging of semi-solid materials.

2. Principle and methods

2.1. Pulse sequence

The multipoint sequence (Fig. 1) is a modification of the SPI sequence. As in SPI, transverse magnetization is

* Corresponding author. Fax: 215-349-5925.
E-mail address: wehrli@oasis.rad.upenn.edu (F.W. Wehrli).

1090-7807/02/$ - see front matter © 2002 Elsevier Science (USA). All rights reserved.
doi:10.1016/S1090-7807(02)00136-2

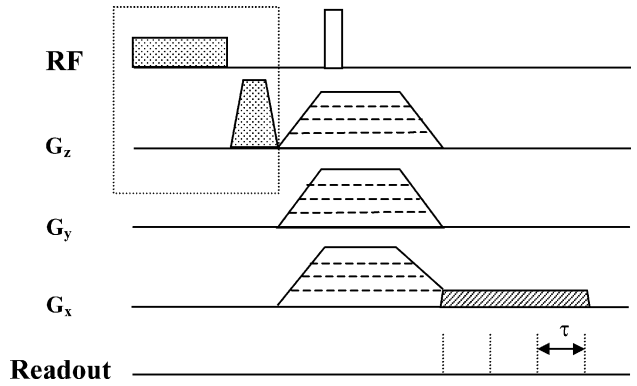

Fig. 1. Multipoint k-space sampling pulse sequence, illustrated for a reduction factor $\mathbf{r} = 4$. Four k-space points are sampled per TR cycle during the extension of the readout gradient (hatched area). The shaded boxes represent a long-T_2 saturation pulse and dephasing gradient, played out before the excitation pulse to saturate the signal from long-T_2 species.

created using a short and strong RF pulse, applied after the gradients are switched on, and spatial encoding is accomplished by means of phase-encoding gradients in three spatial directions [9]. The multipoint sequence achieves a reduction in scan time by a factor of **r**, with respect to SPI, by extending one of the phase-encoding gradients, called hereafter "readout gradient," in time and sampling **r** k-space points per TR cycle, at sampling time intervals, τ. The effective echo time (TE_{eff}), defined here as the interval between the RF pulse and the sampling of the first k-space point, is determined by τ and the ramping time of the gradients (t_{ramp}), which limits the minimally achievable TE_{eff}.

2.2. Sampling scheme and PSF: 1D simulations

Many trajectories are possible during k-space sampling. Among those, two different k-space sampling schemes have been investigated and their effects on image sensitivity and resolution have been studied.

2.2.1. Sequential k-space sampling

In sequential k-space multipoint sampling, **r** successive k-space points are sampled every TR cycle. This is accomplished by using the readout gradient waveforms shown in detail in Fig. 2a, for $\mathbf{r} = 4$. For a given sampling time, τ, the amplitude of the readout gradient extension (G_0) is a function of the field of view (FOV). The step size of the phase-encoding portion of the readout gradient (ΔG) is given by $\Delta G = \mathbf{r}G_0$. The first k-space point is sampled after the gradient ramp, therefore, the time interval between the RF pulse and the beginning of the gradient ramp has been reduced to $\tau - (1/2)t_{\text{ramp}}$, which determines the effective echo time, $TE_{\text{eff}} = \tau + (1/2)t_{\text{ramp}}$. In this manner, the path traveled in k-space during TE_{eff} is incremented by $(\gamma/2\pi)\mathbf{r}G_0\tau$ from step to step, in order to ensure continuous coverage. During the gradient step

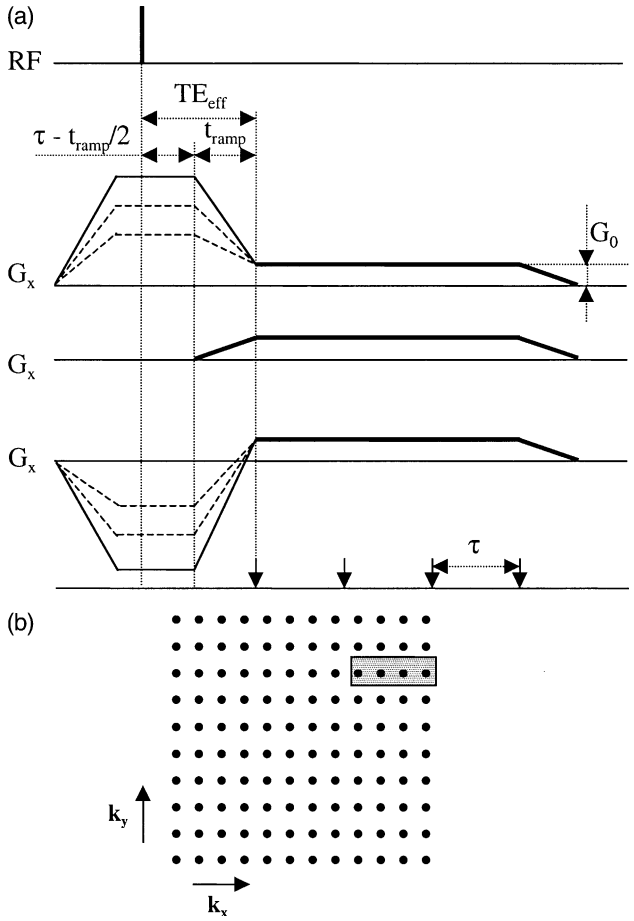

Fig. 2. (a) Readout gradient waveforms for sequential sampling. During the extension of the readout gradient (bold lines), four successive k-space points are sampled for each phase-encoding step (dashed lines). Gradient waveforms shown are used for acquisition of $k_x > 0$ (top), $k_x = 0$ (middle), and $k_x < 0$ (bottom). (b) k-Space trajectory, $\mathbf{r} = 4$, showing the k-space segment acquired during a TR cycle.

of zero gradient strength amplitude, the first k-space point sampled is off the center of k-space by an amount $k_0 = (\gamma/2\pi)(1/2)G_0t_{\text{ramp}}$, due to the readout gradient ramping. Effectively, the whole k-space region sampled in this way is shifted along the k-space readout axis by the same amount k_0. It is possible to ensure the acquisition of the signal for $k = 0$, by setting t_{ramp} and τ so that k_0 is a multiple of the k-space interval, i.e., $k_0 = i\Delta k$, $i =$ integer. This condition is met when $(1/2)t_{\text{ramp}} = i\tau$, which requires t_{ramp} to be a multiple of 2τ. Fig. 2b shows the k-space trajectory for the sequential k-space sampling scheme, where a segment sampled in a single TR is highlighted.

Due to the periodicity of the sampling function (Fig. 3a), the PSF (Fig. 3b) is given by a series of **r** impulses, separated by $N_x/\mathbf{r}$ pixels, where N_x is the total number of acquired points in the readout dimension and **r** is the reduction factor. As a result, ghosts appear in the image domain, in the readout direction, which are replicas of

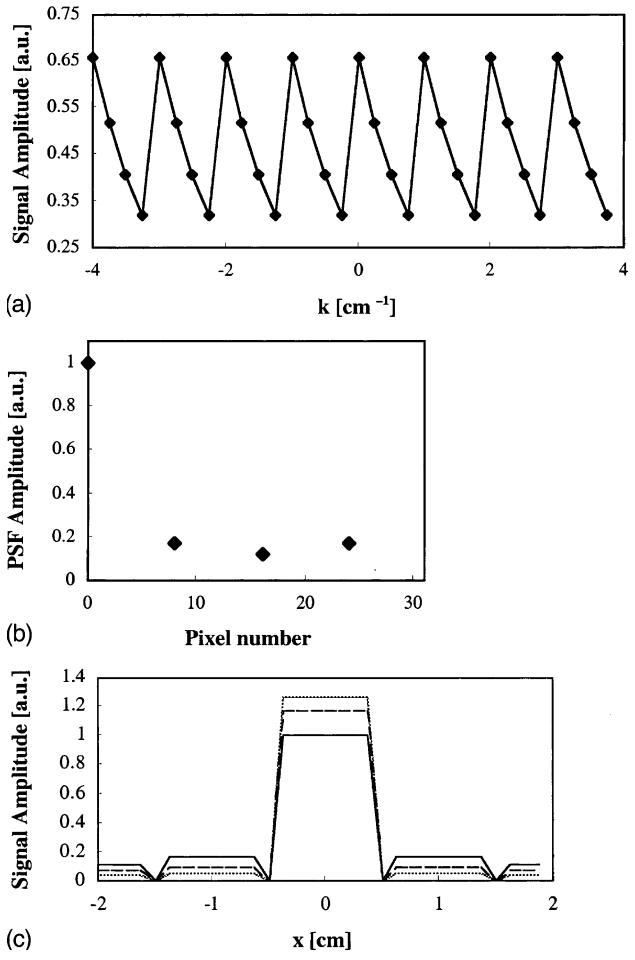

Fig. 3. (a) k-Space sampling function during sequential k-space sampling. (b) PSF. (c) Simulated 1D image. Simulation details: FOV = 4 cm, object length = 0.8 cm, $T_2^* = 250\,\mu s$, $t_{ramp} = 90\,\mu s$, matrix size = 32, $\tau = 60\,\mu s$, $G_0 = 0.98$ G/cm (continuous line), $\tau = 30\,\mu s$, $G_0 = 1.96$ G/cm (dashed line), $\tau = 15\,\mu s$, and $G_0 = 3.92$ (dotted line).

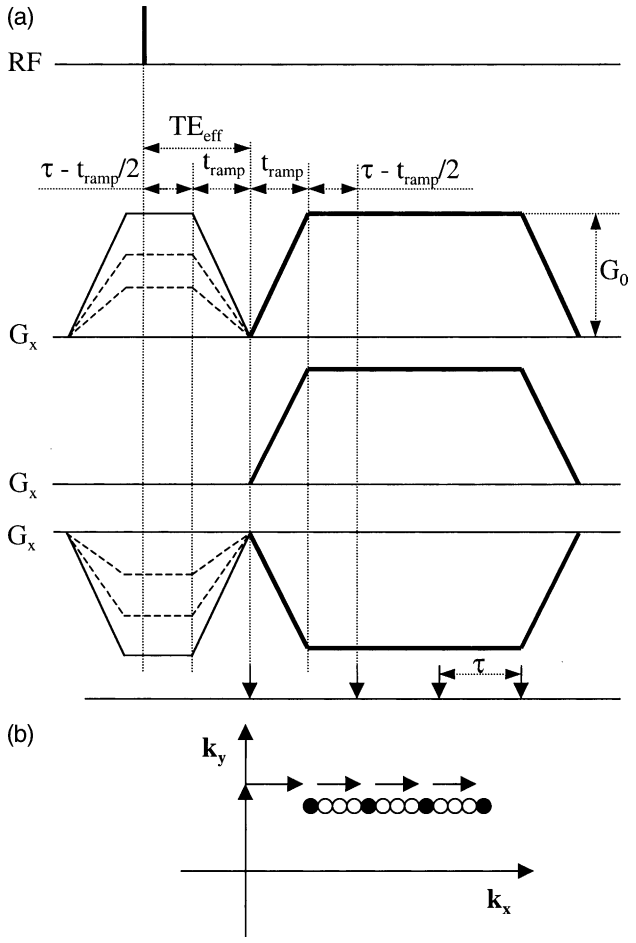

Fig. 4. (a) Readout gradient waveforms for staircase-type k-space sampling, where the readout gradient extension appears in bold lines. Gradient waveforms shown are used for acquisition of $k_x > 0$ (top), $k_x = 0$ (middle), and $k_x < 0$ (bottom). (b) k-Space trajectory, $\mathbf{r} = 4$, showing the four interleaved points acquired in one TR cycle.

the original object, with attenuated intensity, as shown in the simulated 1D image of a rectangular object (Fig. 3c). The intensity ratio of the ghosts to the original image depends on the transverse relaxation decay of the signal (T_2^*) during readout. Accordingly, increasing the strength of the readout gradient extension (G_0) while decreasing the sampling interval attenuates the ghosts while maintaining the same k-space coverage, as demonstrated by the result of the simulations (Fig. 3c).

2.2.2. Staircase k-space sampling

A second k-space sampling strategy, denominated here "staircase sampling" has been investigated. This type of interleaved sampling scheme was first introduced for fast-spin echo sequences [10]. During staircase sampling, the $\mathbf{r}$ k-space points acquired during a TR cycle are separated by a number of k-space intervals equal to $N_x/2\mathbf{r}$. This is achieved by using the gradient waveforms shown in Fig. 4a. In this way, $\mathbf{r}$ blocks of successive k-space signals of equal T_2^* weighting are acquired at both sides of $k = 0$, each block containing $N_x/2\mathbf{r}$ points. In this case, the step size for the phase-encoding portion of the readout gradient (ΔG) and τ define Δk since successive k-space points are sampled after each phase-encoding step during the first acquisition. Therefore, for a given τ, ΔG is determined by the FOV, while the readout gradient extension is given by $G_0 = \pm(N_x/2\mathbf{r})\Delta G$, which corresponds to the strength of the highest gradient step. The readout extension is positive when acquiring the positive half of k_x-space and negative during the acquisition of the negative half. To avoid any shift from the center of k-space, the gradients are switched off to zero amplitude before the first point is acquired and switched on again to G_0 amplitude to acquire the remaining $\mathbf{r} - 1$ points. As in sequential sampling, the acquisition of the first point occurs at $TE_{eff} = \tau + (1/2)t_{ramp}$. The time interval between the acquisition of the first and second points is also equal to TE_{eff}, to maintain a constant k-space sampling interval. Fig. 4b shows the k-space trajectory for $\mathbf{r} = 4$ and the four interleaved points acquired in a TR cycle.

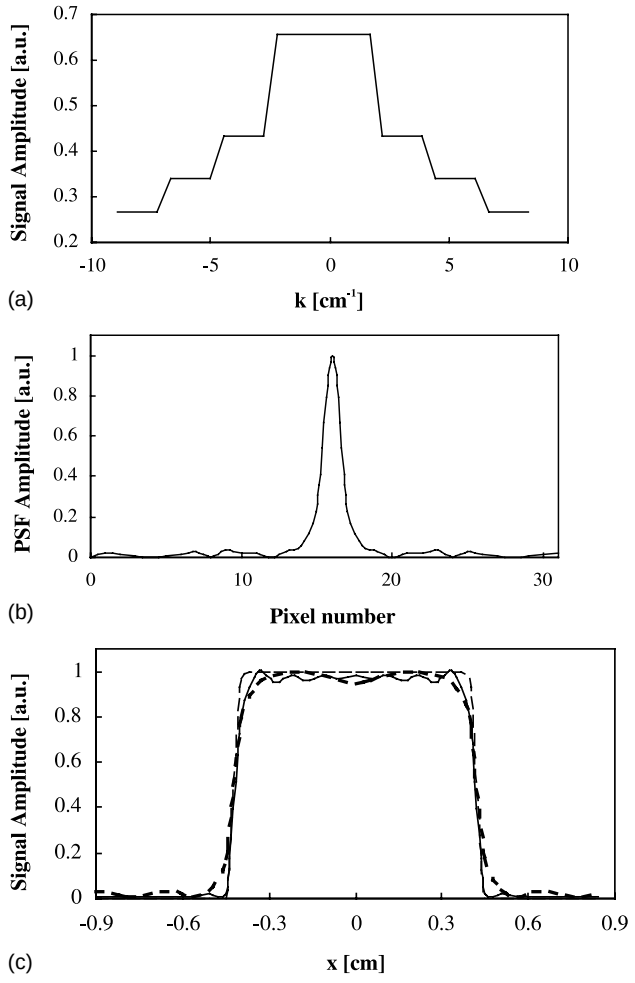

Fig. 5. (a) k-Space sampling function during staircase multipoint sampling. (b) PSF. (c) Simulated 1D image: $N = 32$ (bold, dashed line), $N = 128$ (continuous line), and $N = 512$ (dashed line). Simulation details: FOV = 1.8 cm, object length = 0.8 cm, $T_2^* = 250\,\mu s$, $\tau = 60\,\mu s$, $t_{ramp} = 90\,\mu s$, and matrix size = 32/128/512.

The modulation transfer function (Fig. 5a) is symmetric with respect to the center of k-space resulting in the simulated PSF shown in Fig. 5b. The result of the convolution of the PSF with the original object causes blurring of the image and the discontinuities on the PSF lead to ringing, as shown by the simulated image of a rectangular object (Fig. 5c). Finally, since the k-space points are acquired non-sequentially, the data must be reordered and interleaved during post-processing before Fourier transformation.

2.3. Experiments

The multipoint k-space sampling sequence was implemented on a vertical-bore superconducting spectrometer/micro-imaging system, operating at 9.4 T (DMX-400, Bruker Instruments, Billerica, USA). The system was equipped with water-cooled gradients (maximum gradient strength of 100 G/cm, gradient ramping time of approximately 100 μs). Images were acquired using a 10 mm inner diameter RF coil.

3D images of a cylindrically shaped piece from a Lego toy set were obtained, with both sampling strategies. The relaxation characteristics of this polymer are typical of the materials for the targeted application of the method. The proton spectrum has two broad resonances, assignable to aliphatic and ethylenic protons (data not shown), with line-widths at half-maximum of approximately 1000 Hz (i.e., $T_2^* \approx 300\,\mu s$).

The following imaging parameters were used: TR = 30 ms, flip angle = 36° (optimum for $T_1 = 138$ ms [8]), $\tau = 60\,\mu s$; (a) sequential sampling: RF pulse length (PL) = 3 μs, FOV = $4 \times 4 \times 2$ and $4 \times 2 \times 2\,cm^3$, data matrix = $64(16) \times 64 \times 32$ and $128(32) \times 64 \times 32$, scan time = 16 and 32 min; (b) staircase sampling: PL = 4 μs, FOV = $2\,cm^3$, data matrix = $64(16) \times 64 \times 16$ and $128(32) \times 64 \times 16$, two averages, scan time = 16 and 32 min.

In addition, 3D images of the proximal end of a rat tibia were acquired. For this purpose the bone marrow was removed by immersion in 2.6% sodium hypochlorite in an ultrasonic bath for 30 min, followed by centrifugation at 4000 rmp for 15 min and rinsing with a water jet. The images were collected with the following parameters: TR = 30 ms, PL = 3 μs, flip angle = 25° (optimum for $T_1 = 300$ ms [11]). For sequential sampling: FOV = $3 \times 1.5 \times 1.5\,cm^3$, data matrix = $64(16) \times 32 \times 32$, scan time = 8 min. For staircase sampling: FOV = $1\,cm^3$, data matrix = $32(8) \times 32 \times 16$, two averages, scan time = 4 min.

In order to demonstrate the feasibility of selectively imaging short-T_2 species (matrix-bound bone water) in the presence of signal from long-T_2 protons (bone marrow), a long-T_2 saturation pulse followed by a dephasing gradient was implemented before the excitation pulse (see Fig. 1). This method was first introduced by Pauly et al. [12] and was subsequently analyzed quantitatively by Sussman et al. [13]. The saturation RF pulse flips the long-T_2 magnetization into the transverse plane, while leaving the short-T_2 spins undisturbed. The subsequent gradient applied in the slice-select direction dephases the spins from the long-T_2 species. This preparation cycle precedes the hard excitation pulse which is applied immediately following the spoiler gradient and the data are acquired as previously described. The modified sequence was used to image the shaft of a rabbit tibia that was excised from the animal after euthanasia and kept frozen until the night before the imaging experiment. The shaft was cut from the whole bone and allowed to defrost by maintaining it at room temperature for several hours. 3D images were then acquired with and without the saturation pulse, using the staircase sampling strategy, with the following imaging parameters: TR = 150 ms, PL = 4 μs, flip angle = 24°, FOV = $1 \times 1 \times 3\,cm^3$, data matrix = $64(16) \times 32 \times 16$, scan time = 20 min. The length of the long-T_2 saturation

($\pi/2$) pulse was set to 3840 ms in order to maximize the pulse bandwidth while keeping the ratio of the pulse length to the T_2 of the bone water protons ($\approx$250 μs [11]) greater than 10 to minimize saturation of the short-T_2 species. Since the marrow was predominantly fatty (as seen from the proton spectrum, data not shown), the frequency of the saturation pulse was centered on the methylene resonance. The ratio of the saturation pulse length to the T_2 of fat ($\approx$90 ms [14]) was lower than 0.1, which ensured a high degree of saturation of the fat signal. The dephasing gradient was made contiguous with the z-phase-encoding gradient to minimize gradient switching time.

3. Results and discussion

Fig. 6 shows images of the Lego piece acquired using the MP sequence. The images in Fig. 6a show that sequential k-space sampling results in the predicted ghosts in readout direction (the ghosts do not interfere with the image of the original object since the FOV was chosen to be four times the object thickness). Increasing the strength of the readout gradient extension (G_0) while decreasing the sampling interval attenuates the ghosts while maintaining the same k-space coverage. The image acquired by doubling G_0, shows diminished ghost intensity, since the T_2 modulation of the signal during readout is reduced (second from top in Fig. 6a). Increasing G_0 by another factor of 2 significantly attenuates the artifacts (third image from top). The ghost intensity can be also reduced by PSF deconvolution, which is achieved by dividing the k-space data by the sampling function, constructed from the spectral data. The bottom image in Fig. 6a was reconstructed from the same raw data as the top image after PSF deconvolution, showing significantly reduced ghost intensity. The sampling function can be obtained by acquiring the FID signal at the sampling times of the imaging experiment (i.e., acquiring the signal with all gradients off). The deconvolution process caused a decrease in SNR, which is a problem common to all inverse filters [15]. This method is strictly applicable only to samples with spatially homogeneous T_2. Fig. 6b displays a surface rendering of the object obtained from the 3D data set. Fig. 6c shows images of the same slice in the Lego piece acquired using staircase sampling. The image on the left was windowed to emphasize the ringing and blurring artifacts in the readout direction. The artifacts are attenuated on the right image, which was acquired with increased matrix size in the readout direction. By doubling the matrix size (doubling k-space area), relaxation-induced attenuation of k-space signals is reduced, which corresponds to a narrowing of the PSF and concomitant reduction in blurring as illustrated with the simulation in Fig. 5c. This is an advantage of staircase over sequential

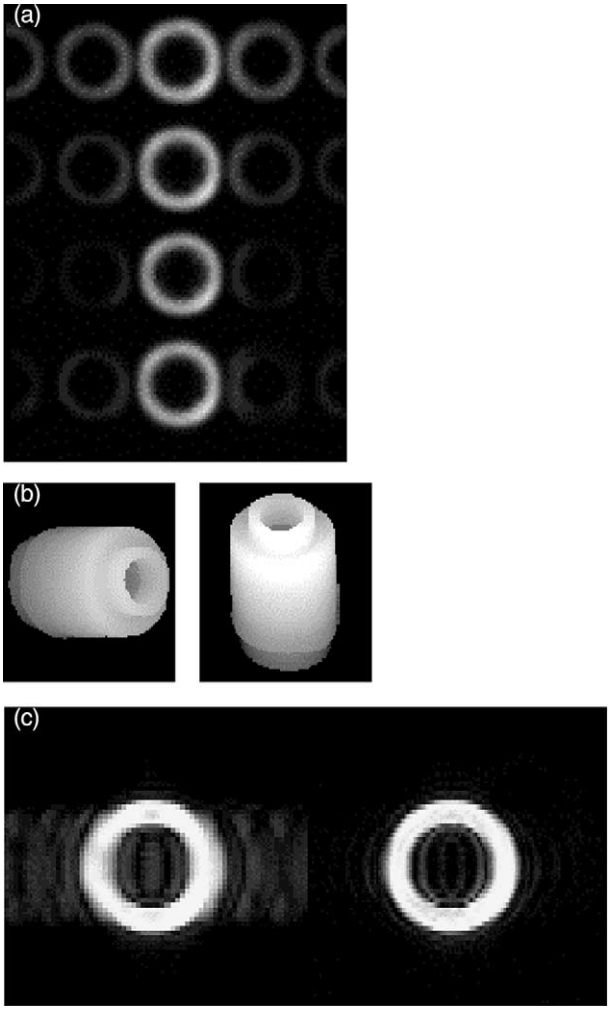

Fig. 6. (a) Center slice of the 3D data set acquired from the Lego piece by sequential multipoint k-space sampling. From top to bottom: (1) $G_0 = \Delta G/4$, $\tau = 60$ μs; (2) $G_0 = \Delta G/2$, $\tau = 30$ μs; (3) $G_0 = \Delta G$, $\tau = 15$ μs; and (4) image reconstructed after deconvolution of the PSF. (b) Surface rendered 3D data set (matrix = $128 \times 64 \times 32$). (c) Same slice from the Lego piece imaged using staircase sampling.

sampling, since for sequential sampling the PSF is not affected by increased matrix size. Ideally we would like the width of the PSF due to the sampling strategy to be less than a pixel, so that the resolution is determined by the size of k-space sampled. The possible contribution from diffusion to the PSF is unlikely to limit the achievable resolution in our targeted application since diffusion in solids (such as in bone) is two orders of magnitude slower than self-diffusion of water [16]. Finally, it is noted that no chemical shift artifacts are present in these images in spite of the fact that the two resonances in the Lego piece spectrum are being excited. The chemical shift difference between these two resonances ($\approx$1600 Hz) causes a discrete phase modulation of the signal. However, the maximum phase spread between the center and the highest k-space frequency is very small compared to the phase spread due to the

imaging gradients, thus not leading to an observable chemical shift artifact.

Multipoint mapping images of the proximal end of a rat tibia are presented in Fig. 7. Fig. 7a shows a slice of the 3D data set acquired using the staircase sampling strategy. 3D projections of the whole sample, created from the 3D data set acquired using the sequential sampling strategy are shown in Fig. 7b. These images of the bone sample were acquired after removal of the marrow.

A major challenge to image tissues with short-T_2 in vivo is the presence of strong signals from the long-T_2 tissues. In the case of bone, both cortical and trabecular, the bone tissue is always adjacent to the bone marrow, which has a much longer T_2 (by over two orders of magnitude) and higher proton density. Therefore, the marrow will appear with greater intensity in the acquired images, as illustrated in Fig. 8a, which is an image of the cross-section of a rabbit tibia diaphysis acquired with the intact marrow using the MP sequence and the staircase sampling strategy. In Fig. 8a, the cortical bone appears with very low intensity, compared with the strong signal intensity of the bone marrow. By contrast, in the image acquired using the long-T_2 saturation pulse, the signal from the cortical bone has been greatly enhanced relative to the signal from the bone marrow (Fig. 8b). There remains residual marrow signal, presumably caused by the presence of hematopoietic marrow (water) which is not suppressed since the narrow-banded saturation pulse was centered on the methylene resonance, thus not saturating the water signal. The use of the saturation pulse allows an increase in receiver gain that results in higher SNR of the cortical bone signal.

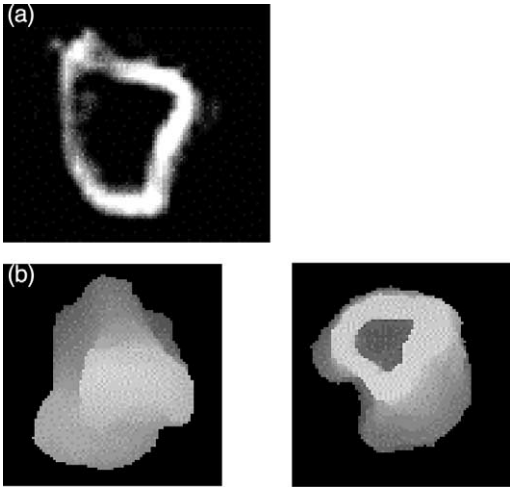

Fig. 7. (a) Center slice of a 3D data set acquired with the MP sequence using the staircase sampling (in-plane pixel size = 312.5 μm, slice thickness = 625 μm, scan time = 4 min) showing a cross-section of the proximal end of a rat tibia. (b) Surface rendered images of the entire specimen, created from the 3D data acquired using the MP technique and sequential sampling (isotropic resolution = 468 μm, scan time = 8 min). The image was obtained after marrow removal.

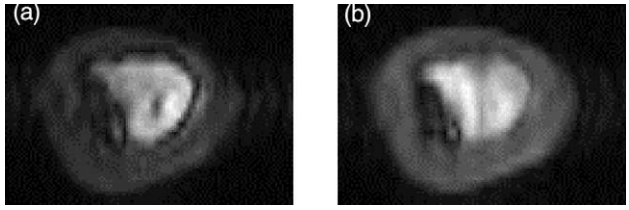

Fig. 8. MP image depicting the cross-section of a rabbit diaphysis obtained in situ with intact marrow, acquired with staircase sampling: (a) without and (b) with saturation of the marrow lipid resonance using a T_2-selective saturation pulse. Attenuation of the marrow signal allows for increased receiver gain resulting in improved SNR of the signal from bone.

T_2-selective RF excitation is a technique for selectively suppressing the signal from long-T_2 protons [12], previously applied to in vivo imaging of tissues with short-T_2 such as articular cartilage and tendon [17]. A limitation of the technique as it has been applied here is the sensitivity of the saturation pulse to B_0 inhomogeneities due to its narrow spectral bandwidth, which also prevents effective saturation of the two spectral components in bone marrow (i.e., fat and water). A modification of this technique has been described [13] that uses a refocusing scheme similar to the spin echo to increase the bandwidth of the saturation pulse, thus reducing its sensitivity to chemical shift. Other technique that could be used for highlighting short-T_2 materials is image subtraction [18]. However, due to the presence of uncorrelated noise in the original and subtracted images, there is a significant loss in contrast to noise ratio. Other problem arising from image subtraction is misregistration when the images are acquired in vivo.

The results in the present work demonstrate the feasibility of imaging short-T_2 materials even in the presence of signal from long-T_2 species. However, the practical implementation of the technique is demanding, since it requires fast switching gradients and large gradient strengths when high resolution is needed. Therefore, this method is not suitable for conventional whole-body imaging where fast and high-amplitude gradients are not usually available. On the other hand, the technique is suited for NMR microscopy of specimens and could possibly be applied to in vivo imaging of small animals.

4. Conclusion

In summary, MP mapping has potential for imaging semi-solid materials with effective transverse relaxation times T_2^* of less than 1 ms more efficiently than its single-point parent. For staircase sampling, increasing matrix size in readout direction was found to be most effective

in reducing *k*-space weighting artifacts. The implementation of a short-T_2 selective RF excitation demonstrates the feasibility of achieving short-T_2 contrast even in the presence of tissues with long-T_2, making the sequence practical for in situ imaging of tissues such as intact bone.

Acknowledgments

The authors are indebted to Dr. M. Takahashi for providing the rat tibia sample and Dr. H.K. Song for helpful discussion.

References

[1] S. Emid, J.H.N. Creyghton, High resolution NMR imaging in solids, Physica B 128 (1985) 81.
[2] D.E. Axelson, A. Kantzas, A. Nauerth, H magnetic resonance imaging of rigid polymeric solids, Solid State Nucl. Magn. Reson. 6 (1996) 309.
[3] S.D. Beyea, B.J. Balcom, T.W. Bremner, P.J. Prado, A.R. Cross, R.L. Armstrong, P.E. Grattan-Bellew, The influence of shrinkage-cracking on the drying behaviour of white Portland cement using single-point imaging (SPI), Solid State Nucl. Magn. Reson. 13 (1998) 93.
[4] Z. Fang, D. Hoepfel, K. Winter, Application of single point imaging (SPI) to solid state materials, Magn. Reson. Imaging 19 (2001) 501.
[5] S.D. Beyea, B.J. Balcom, I.V. Mastikhin, T.W. Bremner, R.L. Armstrong, P.E. Grattan-Bellew, Imaging of heterogeneous materials with a turbo spin echo single-point imaging technique, J. Magn. Reson. 144 (2000) 255.
[6] D.J. McIntyre, F. Hennel, P.G. Morris, SPARE: A robust method for magnetic resonance imaging in inhomogeneous fields, J. Magn. Reson. 130 (1998) 58.
[7] Z.H. Cho, Y.M. Ro, Multipoint *k*-space point mapping (KPM) technique for NMR microscopy, Magn. Reson. Med. 32 (1994) 258.
[8] A. Borthakur, J. Hopkins, R. Reddy, F.W. Wehrli, Segmented readout for microimaging of semi-solid materials and quadrupolar nuclei, in: Proc. ISMRM, Fifth Annual Meeting Vancouver, vol. 3, 1997, p. 2093.
[9] S. Gravina, D.G. Cory, Sensitivity and resolution of constant-time imaging, J. Magn. Reson., Ser. B 104 (1994) 53.
[10] P.S. Melki, R.V. Mulkern, L.P. Panych, F.A. Jolesz, Comparing the FAISE method with conventional dual-echo sequences, J. Magn. Reson. Imaging 1 (1991) 319.
[11] A. Borthakur, R. Reddy, F.W. Wehrli, NMR studies of exchangable hydrogen in bone, in: Proc. ISMRM, Sixth Annual Meeting Sydney, 1998.
[12] J. Pauly, C. Conolly, A. Macovski, Supression of long-T_2 components for short T_2 imaging, in: SMRM, 12th Annual Meeting New York, 1992, p. 145.
[13] M.S. Sussman, J.M. Pauly, G.A. Wright, Design of practical T_2-selective RF excitation (TELEX) pulses, Magn. Reson. Med. 40 (1998) 890.
[14] F. Schick, Bone marrow NMR in vivo, Prog. Nucl. Magn. Reson. Spectrosc. 29 (1996) 169.
[15] K. Oshio, S. Manbir, A computer simulation of T_2 decay effects in echo planar imaging, Magn. Reson. Med. 11 (1989) 389.
[16] M.A. Fernandez-Seara, S.L. Wehrli, F.W. Wehrli, Diffusion of exchangeable water in cortical bone studied by nuclear magnetic resonance, Biophys. J. 82 (2002) 522.
[17] G.E. Gold, D.R. Thedens, J.M. Pauly, K.P. Fechner, G. Bergman, C.F. Beaulieu, A. Macovski, MR imaging of articular cartilage of the knee: new methods using ultrashort TEs, AJR Am. J. Roentgenol. 170 (1998) 1223.
[18] A. MacKay, K. Whittall, J. Adler, D. Li, D. Paty, D. Graeb, In vivo visualization of myelin water in brain by magnetic resonance, Magn. Reson. Med. 31 (1994) 673.